Numerical and experimental investigation into the mechanism of the microbubble drag reduction

Takafumi KAWAMURA

Department of Environmental and Ocean Engineering, the University of Tokyo

7-3-1 Hongo, Bunkyo-ku, Tokyo, 113-8656, JAPAN

Abstract

This paper summarizes the outcome of the five year efforts of the project members towards understanding of the mechanism of the microbubble drag reduction. The experimental investigations can be highlighted by the two achievements. One is the direct measurement of the turbulent statistics in drag reducing flow by use of the PTV/LIF technique, and the other is the identification of the effect of the bubble size. On the other hand, the numerical simulation using the front-tracking method clarified the effect of the Reynolds number on the drag reduction. Microbubbles increase the frictional drag at Re_τ=180 but decrease at Re_τ=1100. In order to explain those results, parametric simulation of a homogeneous turbulent shear flow was carried out, and finally a simple mechanism which can explain all these experimental and numerical results has been presented.

1. Introduction

Many experimental results have confirmed that microbubbles can reduce the frictional drag of a turbulent boundary layer by 20 – 80% [1-3], but there has not been clear explanation how microbubbles reduce the drag. One of the most apparent effects of bubbles is the decrease of the mean density of the mixture. Since the turbulent transport of the momentum is proportional to the fluid density, the reduction of the mixture density contributes to the drag reduction. Another known effect of bubbles is the increase of the effective viscosity. The increase of the viscosity can also decrease the frictional drag by partially re-laminarizing the turbulent flow. Kato et al [4] experimentally confirmed that injection of high-viscosity fluid into a turbulent boundary layer can decrease the frictional drag by up to 50%. However, it can be easily found that these two apparent effects are not sufficient to explain the magnitude of the drag reduction measured in experiments. Figure 1 shows an example of the relation between the bulk void fraction and the measured drag reduction in a fully developed channel flow [5]. The magnitude of the drag reduction at the bulk void fraction of 5% is about 20%, which is much higher than the expected value by considering only the decrease of the mean density and the increase of the effective viscosity. Therefore the modification of the turbulence has to be taken into account to fill the gap. The modification of turbulence was also considered in the early models of drag reduction [6] as reduction of the Reynolds shear stress. However, since the measurement of velocity field in bubbly flow has been very difficult, the turbulence modification has been only a hypothesis.

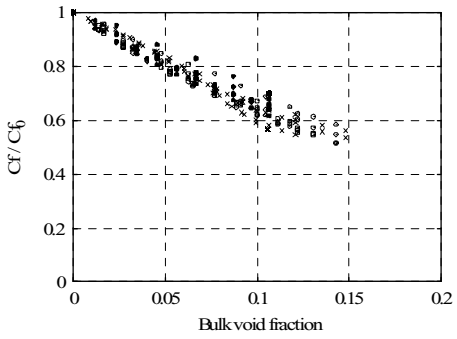

Fig. 1 Typical relation between the bulk void fraction and the drag reduction rate in a channel flow [5]

Meanwhile various experiments were carried out to find out the parameters which determine the drag reduction rate. For example, Guin et al [2] showed that the drag reduction rate is well correlated to the near wall void fraction than to the bulk value; Moriguchi and Kato [5] examined the influence of the bubble diameter on the drag reduction in a fully developed channel flow and found that the drag reduction rate is independent of the average diameter.

Although these measurements of the drag reduction rate suggest that bubbles suppress the turbulent transport of momentum, there has not been direct measurement of the Reynolds stress in bubbly flow due to experimental difficulties. Several researchers tried to explain the turbulence modification by numerical simulation [7-9], but clear explanation of the sustained drag reduction has not been presented yet.

The drag reduction mechanism is not only of scientific interest but also of engineering importance in practical use. Therefore the goal of the microbubble team of the "*Smart Control of Turbulence*" project has been to improve the efficiency of the microbubble drag reduction through clear understanding of the physical mechanism.

Both experiments and numerical simulations played indispensable roles in this project. The experiments provided quantitative evidences of the drag reduction and the turbulence modification, while parametric simulations quantitatively explained the underlying mechanism. This paper summarizes the outcome of the work with respect to the understanding of the drag reduction mechanism.

2. Experimental evidences

The experimental investigations focused on the direct measurement of the turbulence modulation and on the identification of the parameters which influence the drag reduction rate. The measurements of the local skin friction were carried out for fully developed channel flows, spatially developing boundary layer flow in a channel, and the 50m flat plate model.

Figure 2 shows the one of the most important results. It was shown by Moriguchi and Kato [5] that the drag reduction rate in a fully developed channel flow does not depend on the average diameter within the range between 0.5 and 2.0mm. However, it was also found that the bubble size does influence the drag reduction in an external flow through changing the distribution of the void fraction. Figure 3 shows the measured void fraction profiles for different bubble diameters [10]. It is noted that small bubbles are dispersed faster, while large bubbles remain near the wall due to the buoyancy. Figures 4 and 5 both show the magnitude of the drag reduction at different freestream velocities. The drag reduction rate does not depend on the freestream velocity in the fully developed channel flow but it does depend in the spatially developing external boundary layer flow. The increase of the freestream velocity decreases the bubble size and the relative importance of the buoyancy by increasing the inertial force. It is supposed that the void fraction profile in the external flow is drastically changed by the increased velocity, while this effect is not significant in a fully developed channel flow.

Another experimental achievement to mention is the direct measurement of the velocity field in bubbly flows by use of the PTV/LIF technique [11]. The measurement technique first threw light on the modulation of turbulence by bubbles in the drag reducing flow.

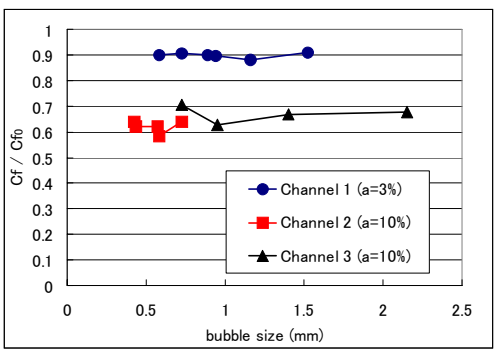

Fig. 2 Drag reduction rate versus the average bubble diameter in a fully developed channel flow [5]

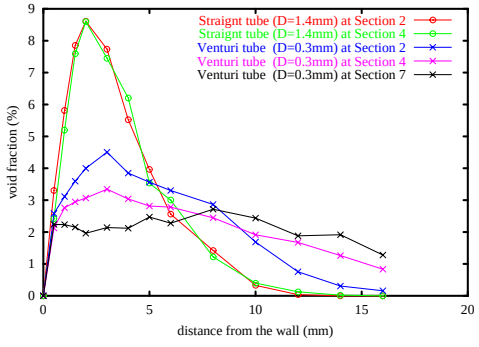

Fig. 3 Measured void fraction profiles in a spatially developing boundary layer flow for different average bubble diameters [10]

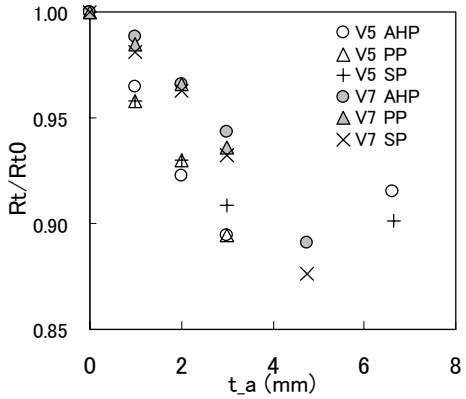

Fig. 4 Measured total drag reduction versus the apparent air layer thickness for the towed 50m flat plate [10]. V5 and V7 are for the freestream velocity of 5 and 7 m/s, respectively.

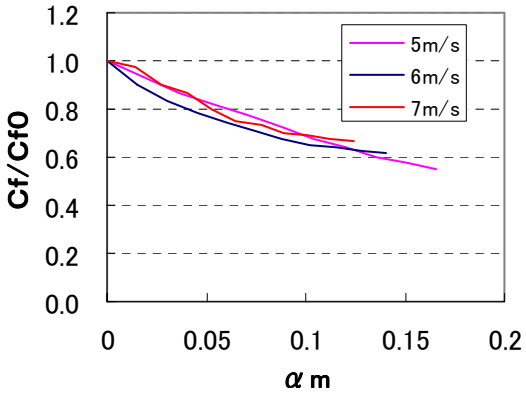

Fig. 5 Measured local skin friction reduction versus the bulk void fraction in a fully developed channel flow at different mean velocities [5]

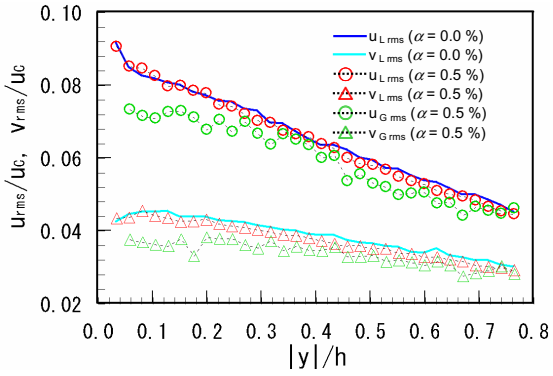

Fig. 6 PTV measurement of the streamwise and wall-normal components of the turbulent intensities in single phase and bubbly flows [11]

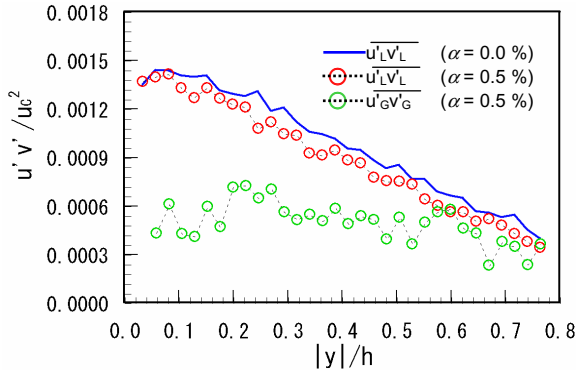

Fig. 7 PTV measurement of the Reynolds stress in single phase and bubbly flows [11]

Figure 6 shows the measured turbulent intensities in the single phase and bubbly flows. The subscript L denotes the value in the liquid phase, and G denotes the value of the centroid of the bubbles. The streamwise component u_{Lrms} in bubbly flow is almost the same as that in the single phase flow, but the wall-normal component v_{Lrms} is clearly decreased by the presence of bubbles. The magnitude of the turbulent intensity of bubbles is smaller than that of the liquid phase meaning that bubbles do not move as hard as a liquid element due to their finite size. These results suggest that the directional redistribution of the turbulent kinetic energy is suppressed by relatively slow-moving bubbles occupying the space. Probably as a result, the Reynolds stress is decreased as shown in Fig. 7.

3. Simulation of channel flow

At first, the numerical simulation aimed at reproducing the drag reduction measured in the experiments. The early trials for low Reynolds number channel (Re_τ=180) flow were unsuccessful [12-13], but later drag reduction was confirmed in the simulation of the high Reynolds number channel flow (Re_τ=1100) [14].

Several different methods for resolving the interaction between bubbles and turbulence were used. One is the front-tracking approach [12] which satisfies the dynamic and kinematic boundary conditions of the gas-liquid interface at the exact location of the deformed bubble surface. Other methods for treating solid particles of finite size [13] were also used for comparison.

Figure 8 shows the time history of the friction coefficient in the DNS of a fully developed channel flow at Re_τ=180 [12]. It is shown that the frictional drag is significantly increased by the introduction of bubbles. Since it is difficult to realize the same condition, this increase of the frictional drag at a low Reynolds

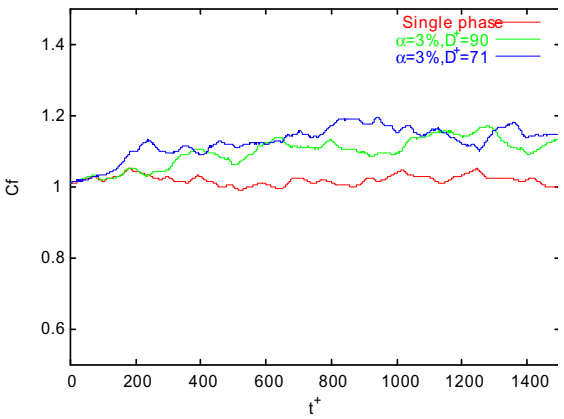

Fig. 8 Time history of the friction coefficient in the DNS of channel flow at Re_τ=180 [12]

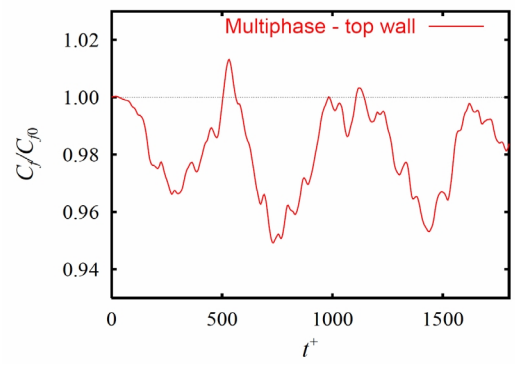

Fig. 9 Time history of the relative friction coefficient of the bubbly flow to the single phase flow in the LES of channel flow at Re_τ=1100 [14]

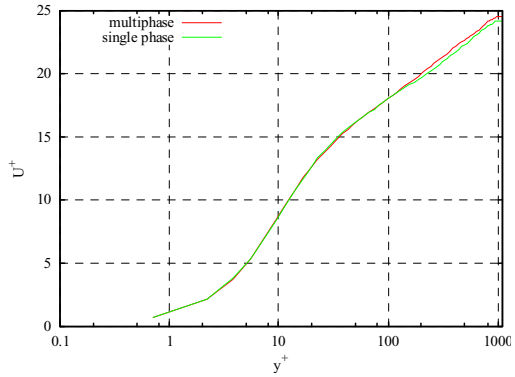

Fig. 10 Mean velocity profiles in single phase and bubbly channel flows at Re_τ=1100 [14]

number has not been experimentally confirmed. However, considering that consistent results were obtained by a numerical simulation using different methods [13], this tendency is supposed to be true.

In order to confirm the Reynolds number effect, LES of bubbly channel flow at Re_τ=1100, which is close to the value in the experiment of Moriguchi and Kato [5], was carried out [14]. As shown in Fig. 9, reduction of the frictional drag was finally confirmed in the simulation. The obtained turbulent statistics were similar to the PTV measurement, and it is supposed that essentially the same phenomenon as in the experiment was reproduced in the LES.

The comparison of the mean velocity profiles in the single and bubbly flows shown in Fig. 10 indicates that the mean velocity in the bubbly flow is smaller than in the single phase flow in the region near the wall ($y^+ < 200$) but larger in the region far from the wall ($y^+ > 200$). This means that the reduction of the frictional drag is due to the increase of the mean velocity in the outer region. From this fact, a hypothesis can be set up that the bubbles decrease the Reynolds stress in the outer region where the mean velocity gradient is small, while they increase the Reynolds stress in the near wall region where the mean velocity gradient is large. This hypothesis can explain the increase of the friction coefficient in the low Reynolds number channel flow in which the outer region does not exist.

4. Simulation of homogeneous shear flow

The results of the channel flow simulations suggest that the presence of bubbles can either decrease or increase the Reynolds stress depending on certain condition. As a tool to confirm this hypothesis, the simulation of channel flow is not suitable in two aspects: one is the computational cost and the other is that the presumed dominant parameters vary with the distance to the wall. In order to solve these two problems, homogeneous turbulent shear flow was investigated [15]. The homogenous turbulent shear flow is a uniformly sheared flow as defined in Fig. 11.

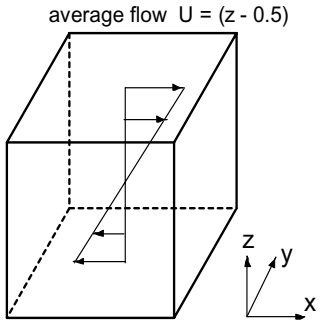

Fig. 11 Definition of the homogeneous turbulent shear flow

The important parameters in this flow are the shear Reynolds number Re and the turbulent Reynolds number Re_t, which are define as follows:

$$\mathrm{Re} = \frac{Sd^2}{\nu} \tag{1}$$

and

$$\mathrm{Re}_t = \frac{u_{rms} d}{\nu} \tag{2}$$

in which S is the shear rate, d is the equivalent bubble diameter, and u_{rms} is the root mean square velocity fluctuation. The shear Reynolds number Re indicates the magnitude of the mean velocity gradient, while the turbulent Reynolds number Re_t is the measure of the turbulent intensity. It should be noted that the shear Reynolds number is a given parameter, while the turbulent Reynolds number varies with the growth or decay of the turbulence. If the surface energy is ignored, the budget of the turbulent kinetic energy K can be written as

$$\dot{K} = P - \varepsilon \tag{3}$$

where P is the production term

$$P = -S\overline{uw} \tag{4}$$

The simulations were performed for different shear Reynolds numbers and initial turbulent Reynolds numbers, and the changes of the production P and the dissipation ε with respect to the values in the single phase flow are discussed.

Figures 12 and 13 show the normalized production of the turbulent kinetic energy at Re=581, and Re=2326 respectively. The turbulent Reynolds number Re_t is also different. The presence of bubbles increases the production at Re=581, and decreases at Re=2326. Figure 14 and 15 show the normalized dissipation of the turbulent kinetic energy at Re=581, and Re=2326 respectively. Unlike the

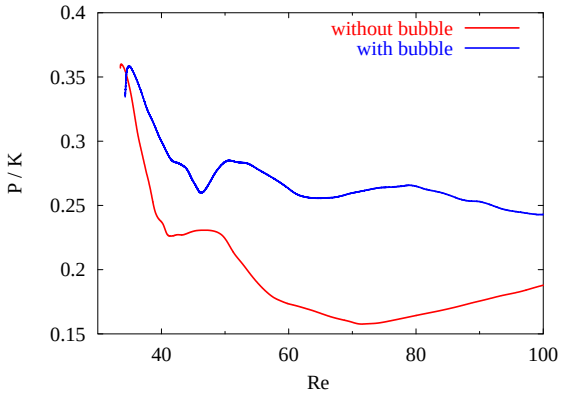

Fig. 12 Normalized production of turbulent kinetic energy in the homogeneous shear flow at Re=581

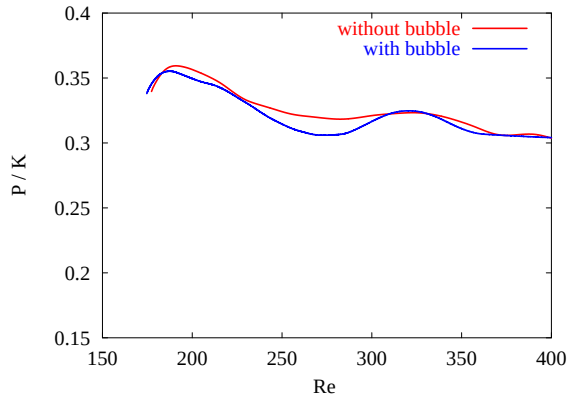

Fig.13 Normalized production of turbulent kinetic energy in the homogeneous shear flow at Re=2326

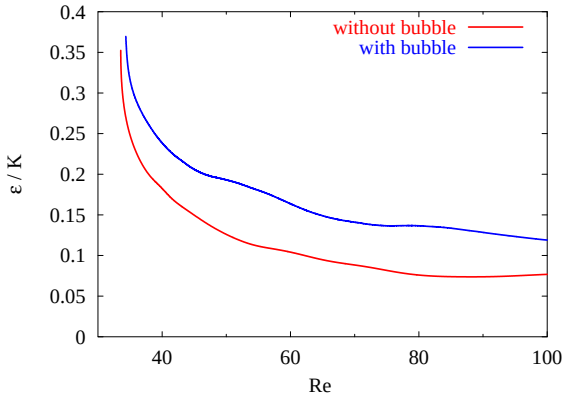

Fig. 14 Normalized dissipation of turbulent kinetic energy in the homogeneous shear flow at Re=581

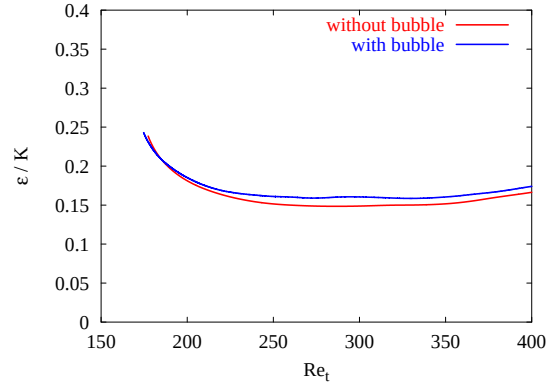

Fig. 15 Normalized dissipation of turbulent kinetic energy in the homogeneous shear flow at Re=2326

production, the dissipation is increased in both cases, but the changes are smaller than in the production. As a result the growth rate of the turbulent kinetic energy is increased at Re=581 and decreased at Re=2326. The decrease of the growth rate can be translated to the reduction of the frictional drag in the channel flow.

The vortex structures visualized by contour surfaces of the second invariant of the velocity gradient tensor shown in Figures 16-19 indicate the different situations at Re=581 and Re=2326. At Re=581, in which bubbles increased the growth rate of the turbulent kinetic energy, strong organized vortices are formed in the wake of bubbles, while such structure is not present at Re=2326, in which bubbles decreased the growth rate. From the observation of the vortex structure at Re=581, the increase of the production by bubbles is supposed to be caused by the interaction between the bubbles and the mean velocity gradient. On the other hand, the figure for Re=2326 show that vortex structures are finer and rather independent of bubbles. In this case, the decrease in the production of turbulent kinetic energy is probably explained by the decreased freedom for turbulent structures to spatially develop. From the dimensional analysis and an assumption that the drag coefficient is in inverse proportion to the shear Reynolds number, the production added by bubbles is estimated to be proportional to

$$P_b = \frac{1}{\mathrm{Re}} \frac{\rho (Sd)^2}{d} \times (Sd) \tag{5}$$

For bubbles to decrease the production, this added production must be much smaller than the underlying production $P = -S\overline{uw}$, thus a new index, which determines whether bubbles increase or decrease the production, can be defined by P / P_b. By using u_{rms}^2 in place of $-\overline{uw}$, the following relation is derived.

$$P / P_b \propto \mathrm{Re}_t^2 / \mathrm{Re} \tag{6}$$

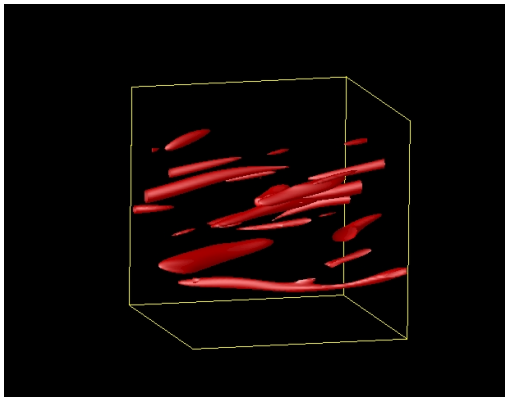

Fig. 16 Vortex structures visualized by contour surfaces of the second invariant of the velocity gradient tensor Q at Re=581 without bubbles.

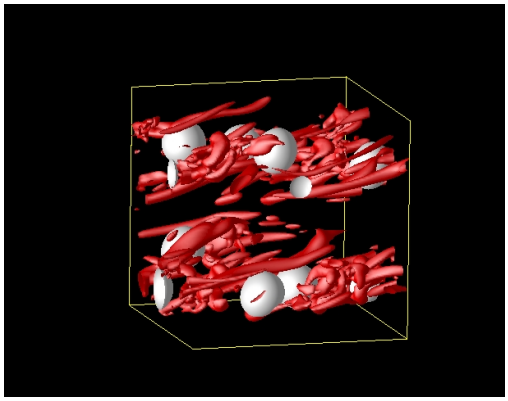

Fig. 17 Vortex structures visualized by contour surfaces of the second invariant of the velocity gradient tensor Q at Re=581 with eight bubbles (α=3.35%)

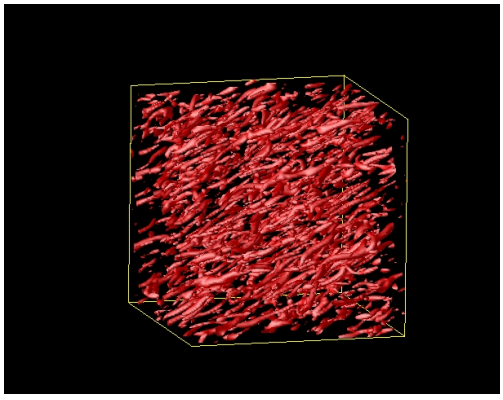

Fig. 18 Vortex structures visualized by contour surfaces of the second invariant of the velocity gradient tensor Q at Re=2326 without bubbles.

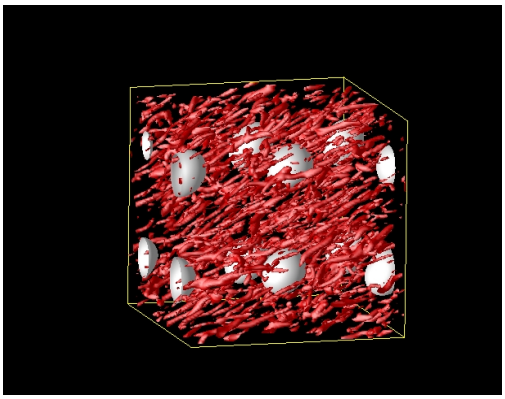

Fig. 19 Vortex structures visualized by contour surfaces of the second invariant of the velocity gradient tensor Q at Re=2326 with eight bubbles (α=3.35%)

By taking the square root of Eq (6), a new parameter is define as follows.

$$R = \mathrm{Re}_t / \sqrt{\mathrm{Re}} \qquad (7)$$

The parameter R is the indication of the turbulent intensity relative to the mean velocity gradient. Figure 20 shows the change of the production by bubbles versus the turbulent Reynolds number Re_t. It is noted that bubbles decrease the production as Re_t is increased, and that increase of the shear Reynolds number increases the production rate. Figure 21 shows the same value versus the new parameter R. Compared with Figure 20, a better correlation is confirmed. The change of the growth rate in Fig. 22 shows the negative values of the growth rate change, which is translated to drag reduction in channel flow, are observed when R is large.

The hypothesis about the parameter R can also explain the different tendencies found in the simulation of channel flow at Re_τ=180 and Re_τ=1100. As shown in Fig. 23, the value of the R parameter is a factor of 2 larger at Re_τ=1100 than at Re_τ=180. Moreover, R does not depend on the bubble diameter. This is important to be consistent with the experimental evidence that the bubble diameter is not important.

5. Conclusion

Based on the experimental evidences and the results of the numerical simulations, a new hypothetical mechanism of the microbubble drag reduction has been presented. The proposed mechanism consists of the following ideas.

1. Bubbles have two effects on the turbulence: One is to enhance the turbulence through additional production, and the other is to suppress the turbulence by decreasing the spatial freedom.
2. The relation between the Reynolds stress and the mean velocity gradient governs the ratio of the suppression effect to the enhancing effect.

This model is consistent with the experimental results that the drag reduction is independent of the bubble diameter and the result of the numerical simulation in which the drag is increased at low Reynolds number and decreased at high Reynolds number.

Although more detailed studies are necessary for validation, the parametric change

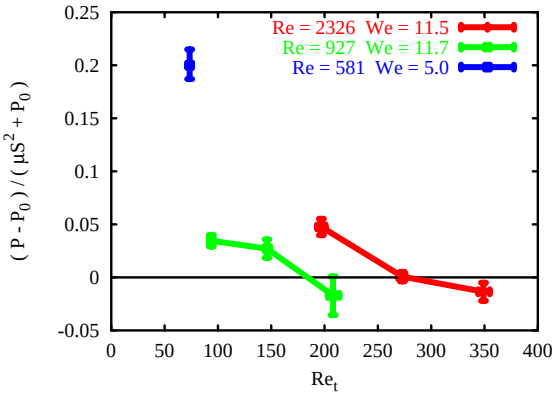

Fig. 20 The change of the production of turbulent kinetic energy by bubbles versus the turbulent Reynolds number Re_τ

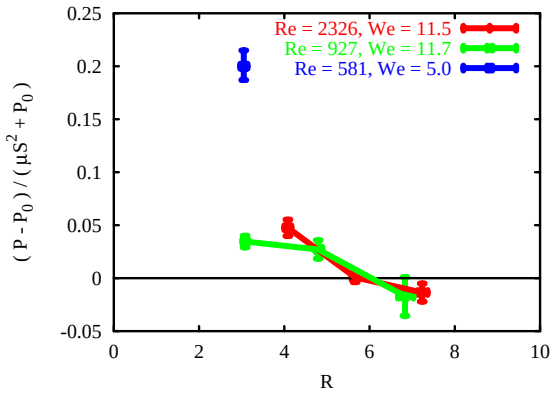

Fig. 21 The change of the production of turbulent kinetic energy by bubbles versus the parameter $R = \mathrm{Re}_\tau / \sqrt{\mathrm{Re}}$

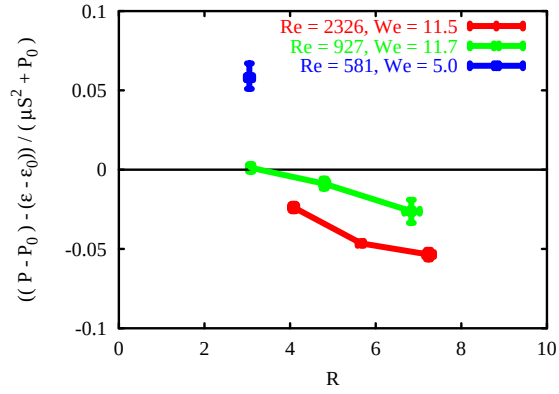

Fig. 22 The change of the growth rate of turbulent kinetic energy by bubbles versus the parameter $R = \mathrm{Re}_\tau / \sqrt{\mathrm{Re}}$

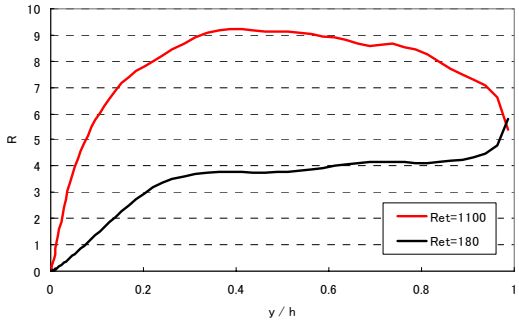

Fig. 23 Profiles of the parameter *R* in the channel flow at Re_τ=180 and Re_τ=1100

of the production and dissipation of turbulent kinetic energy can be easily put into RANS turbulence models to construct a rational tool to predict the microbubble drag reduction.

Acknowledgement

This paper is the summary of the work by the microbubble team of the "Smart Control of Turbulence" project. Their contribution is greatly appreciated.

References

[1] Madavan NK, Deutsch S, Merkle CL (1984) Reduction of turbulent skin friction by microbubbles. Phys Fluids 27:356-363

[2] Guin MM, Kato H, Yamaguchi H et al (1996) Reduction of skin friction by microbubbles and its relation with near-wall bubble concentration in a channel. J Mar Sci Technol 1:241-254

[3] Kato H, Miura K, Yamaguchi H et al (1998) Experimental study on the microbubble ejection method for frictional drag reduction. J Mar Sci Technol 3:122-129

[4] Kato H, Fujii Y, Yamaguchi H et al (1989) Frictional Drag Reduction by Injecting High-Viscosity Fluid. J Soc Naval Arch Japan 168:39-50

[5] Moriguchi, Y., and Kato, H. (2002) Influence of microbubble diameter and distribution on frictional resistance reduction. J. Marine Science and Technology, Vol.7 No. 2, pp. 79 – 85

[6] Legner, HH (1984) A simple model for gas bubble drag reduction. Phys. Fluids, 27:2788–2790

[7] Xu, J., Maxey, M.R. and Karniadakis, G.E. (2002) DNS of turbulent drag reduction using micro-bubbles, J. Fluid Mech. 468, 271-281.

[8] Ferrante, A. and Elghobashi, S., (2004) On the physical mechanisms of drag reduction in a spatially-developing turbulent boundary layer laden with microbubbles, J. Fluid Mech., 503, 345-355.

[9] Lu, J., Fernandez, A. and Tryggvason, G., (2004) The effect of bubbles on the wall shear in a turbulent channel flow, Phys. Fluids (to appear).

[10] Kawamura T, Fujiwara A, et al (2004) The Effects of the Bubble Size on the Bubble Dispersion and Skin Friction Reduction, Proc. of 5th Symp. on Smart Control of Turbulence, The Univ. of Tokyo, Tokyo, Japan, 145-151.

[11] Kitagawa, A., Hishida, K. and Kodama, Y. (2004) Two-phase turbulence structure in a microbubble channel flow, Proc. of 5th Symp. on Smart Control of Turbulence, The Univ. of Tokyo, Tokyo, Japan, 135-144.

[12] Kawamura, T. and Kodama, Y. (2002) Numerical simulation method to resolve interactions between bubbles and turbulence, Int. J. Heat and Fluid Flow, 23, 627-638.

[13] Sugiyama, K., Kawamura, T., Takagi, S. and Matsumoto, Y. (2003) Numerical simulation of transient microbubble flow, Proc. of 4th Symp. on Smart Control of Turbulence, The Univ. of Tokyo, Tokyo, Japan, 51-60.

[14] Sugiyama, K., Kawamura, T., Takagi, S. and Matsumoto, Y. (2004) The Reynolds number effect on the microbubble drag reduction, Proc. of 5th Symp. on Smart Control of Turbulence, The Univ. of Tokyo, Tokyo, Japan, 31-43.

[15] Sugiyama, K., Kawamura, T., Takagi, S. and Matsumoto, Y. (2005) Recent Progress of Microbubble Flow Simulation for Elucidating Drag Reduction Mechanism, Proc. of 6th Symp. on Smart Control of Turbulence, The Univ. of Tokyo, Tokyo, Japan